HOSTED BY
ELSEVIER
Available online at www.sciencedirect.com
ScienceDirect
Soils and Foundations 60 (2020) 327–341
www.elsevier.com/locate/sandf

Technical Paper

A pore water pressure model calibration based on in-situ test results

Anna Chiaradonna [a,*], Alessandro Flora [b], Anna d'Onofrio [b], Emilio Bilotta [b]

[a] Department of Civil, Construction-Architectural and Environmental Engineering, University of L'Aquila, Italy
[b] Department of Civil, Architectural and Environmental Engineering, University of Napoli Federico II, Naples, Italy

Received 6 December 2018; received in revised form 21 December 2019; accepted 26 December 2019
Available online 25 February 2020

Abstract

This paper proposes a procedure for the calibration of a simplified pore water pressure model implemented in 1D effective stress dynamic analyses. The calibration procedure is based on the cyclic strength of the soils as quantified using empirical correlations with in-situ tests, CPT and SPT. Specific relationships have been directly defined among the parameters of the pore water pressure model and the results of in-situ tests. All the steps for the definition of these relationships are described in detail.

The proposed calibration procedure has been used to simulate the seismic response of two well-documented reclaimed sites where widespread liquefaction occurred: Port Island, in Kobe (Japan) and Treasure Island in California (US), struck by the 1995 Kobe and the 1989 Loma Prieta earthquakes, respectively. The results of the analyses have been compared to the actual site response as recorded by downhole acceleration arrays, showing that the proposed approach leads to a good estimate of the site response. Guidelines for calibration of the proposed model are finally provided, and the advantages and limitations of its use are discussed in detail.

Keywords: Liquefaction; Excess pore pressure; Model calibration; In-situ testing; 1D seismic soil response

1. Introduction

Liquefaction has caused significant damage to engineered structures and lifelines during recent earthquakes (2011 Christchurch, New Zealand earthquake; 2012 Emilia, Italy earthquake; 2018 Palu, Indonesia earthquake). An accurate prediction of excess pore pressure build-up induced by seismic action is therefore a fundamental requirement for assessing the seismic safety and resilience of structures and infrastructures in saturated soils.

A reliable prediction of liquefaction usually requires effective-stress site response analyses to be performed. Within this framework, two distinct approaches can be adopted to predict earthquake-induced pore pressures:

(1) a 'loosely coupled' approach in which pore water pressure, pwp, generation is calculated using semi-empirical models and the effects of pwp generation and cyclic degradation are included by degradation of soil strength and stiffness; (2) a 'fully coupled' approach in which the formulation of the constitutive law is developed in effective-stress space, and pwp is computed as the difference between effective-stresses and total stresses in the domain of interest (Matasovic and Hashash, 2012).

Following the 'fully coupled' approach, various nonlinear elastoplastic soil constitutive models have been developed by several researchers, e.g., Prevost, 1985; Beaty and Byrne, 1998; Elgamal et al., 2002; Dafalias and Manzari, 2004; Boulanger and Ziotopoulou, 2015. These models require a number of parameters to characterize

Peer review under responsibility of The Japanese Geotechnical Society.
* Corresponding author at: Department of Civil, Construction-Architectural and Environmental Engineering, University of L'Aquila, Piazzale Ernesto Pontieri, 1, 67040 Monteluco di, Roio (AQ), Italy.
E-mail addresses: anna.chiaradonna1@univaq.it (A. Chiaradonna), flora@unina.it (A. Flora), donofrio@unina.it (A. d'Onofrio), bilotta@unina.it (E. Bilotta).

https://doi.org/10.1016/j.sandf.2019.12.010
0038-0806/

the response of granular soils undergoing elastic or elasto-plastic deformations as well as common features in soils susceptible to liquefaction, e.g., accumulation of volumetric strains under cyclic shear, dilation at large shear strains, excess pore-pressure generation, and dependency of dilatancy on fabric history (Ramirez et al., 2018).

Although widespread in research, the use of these advanced constitutive models in geotechnical engineering practice is currently limited because most of them require a rigorous calibration of a relatively large number of parameters (Ramirez et al., 2018). There are, however, some recently developed models designed to capture the broad range of responses through a relatively easy calibration. The 'loosely coupled' approach adopts semi-empirical pore pressure generation models and is implemented for one-dimensional effective stress dynamic analyses. This model is frequently implemented in 1D codes suitable for effective stress analyses (e.g., DESRA-2 (Lee et al., 1978); D-MOD2000 (Matasovic and Ordonez, 2011); DEEPSOIL (Hashash et al., 2016)).

This second approach is definitely simpler and more accessible to practitioners than the 'fully coupled' one. However, for most of the pore water pressure models, the major limitation is the need to use the cyclic resistance curve requiring the need to define an equivalent number of cycles to represent earthquake shaking (Hashash et al., 2010).

In this framework, Chiaradonna et al., 2018 proposed a simplified pore water pressure model which permits to synthetically express the seismic demand relevant to an irregular time-history of shear stress, and to compare it to the cyclic strength of liquefiable soils, as measured in stress-controlled cyclic laboratory tests, thus avoiding the evaluation of the number of equivalent uniform stress cycles. This simplified model is already implemented in the 1D non-linear code SCOSSA (Tropeano et al., 2016; Chiaradonna et al., 2016) and validated on centrifuge tests and well-instrumented test sites, as detailed in Tropeano et al. (2019) and Chiaradonna et al. (2018b). Currently, the pore water pressure model is based on the cyclic resistance of liquefiable soils as obtained in the laboratory through cyclic triaxial or simple shear tests (Chiaradonna et al., 2018).

In order to extend the applicability of the model to large-scale studies, where laboratory data are often not available, in this paper it is shown that the the parameters of the model can be directly calibrated from the results of conventional in-situ testing (i.e., CPT and SPT).

To do so, after a brief description of the adopted methodology for effective stress analysis (Section 2), the procedure for defining the cyclic strength of soils using empirical correlations with in-situ testing is described (Section 3).

The described procedure is then applied to two well-documented liquefaction cases histories, and the results are compared with acceleration time histories recorded at both sites (Section 4). The results are then discussed and final recommendations are provided (Section 5).

2. The simplified pore pressure model for effective stress analysis

A simplified pore water pressure model, here called 'PWP model' (Chiaradonna, 2016; Chiaradonna et al., 2018; 2019) was implemented in the non-linear code SCOSSA which models the soil profile as a system of consistent lumped masses, connected by viscous dampers and springs with hysteretic behaviour (Tropeano et al., 2016; 2019). The non-linear shear stress-strain relationship is described by the MKZ model (Kondner and Zelasko, 1963) and the modified Masing rules (Phillips and Hashash, 2009). The code permits to select both options of total and effective stress analyses. In this latter case, the effective-stress site response analysis is carried out following a "loosely coupled" approach where a soil constitutive model in total stress is adopted in combination with a semi-empirical model for the prediction of pore pressure build-up and dissipation.

To take into account the pore pressure build-up, the stress-strain relationship of the MKZ model is modified according to the suggestion proposed by Matasovic and Vucetic (1993). The resulting backbone curve is described as follows:

$$F_{bb}(\gamma) = \frac{\sqrt{1-r_u}\, G_0\, \gamma}{1+\beta\left(\frac{\gamma}{\gamma_r}\frac{\sqrt{1-r_u}}{1-r_u{}^{\mu}}\right)^{s'}} \tag{1}$$

where γ is the shear strain level, G_0 is the initial shear modulus, γ_r is the reference shear strain, β and s' are two dimensionless factors, r_u is the excess pore water pressure ratio (i.e., the excess pore water pressure normalized by the initial effective vertical stress) and μ is an exponential constant which expresses the sensitivity of the backbone curve to pore water pressure changes, generally ranging between 3.5 and 5. The same relationship between shear modulus and excess pore water pressure is also frequently used in other codes suitable for effective stress analyses (e.g., Matasovic and Ordonez, 2011; Lee and Finn, 1978).

In perfectly undrained conditions, the excess pore pressure build-up is predicted by the 'PWP model' (Chiaradonna et al., 2018), which makes it possible to compare the irregular time-history of shear stress induced by an earthquake with soil liquefaction resistance, as evaluated in stress-controlled cyclic laboratory tests. The comparison is expressed through the so-called 'damage parameter', κ, which is a function of the undrained cyclic strength curve and is defined as an increasing variable of the applied loading history. Cyclic strength is expressed in terms of a cyclic resistance curve, which univocally relates the number of cycles at liquefaction, N_L, to the cyclic resistance ratio, CRR (the ratio between peak shear stress amplitude, τ_{max}, that induces liquefaction at a given number of cycles and

the initial effective stress, σ'_0). The model analytically describes the cyclic resistance curve by the following equation:

$$\frac{(CRR - CSR_t)}{(CSR_r - CSR_t)} = \left(\frac{N_r}{N_L}\right)^{\frac{1}{\alpha}} \tag{2}$$

where (N_r, CSR_r) is a reference point, CSR_t the asymptotic value of CRR as the number of cycles tends to infinite and α is the slope of the best-fit relationship in a log–log scale (Fig. 1a).

The parameters CSR_t and α are used to compute the damage parameter, κ, for any loading pattern. For a regular harmonic loading of a given amplitude, CSR, i.e., $|\tau_{max}|/\sigma'_0$, κ is proportional to the number of cycles, N, and it can be written as:

$$\kappa = 4N\,(CSR - CSR_t)^{\alpha} \tag{3}$$

The physical meaning of k can be easily deduced from Eq. (3), since it expresses the cumulative damage occurring along the stress path every time the amplitude of the applied stress ratio exceeds the CSR_t threshold value.

Combining Eqs. (2) and (3), the damage parameter at liquefaction, κ_L, can be expressed as follows:

$$\kappa_L = 4\,N_r\,(CSR_r - CSR_t)^{\alpha} \tag{4}$$

The pore pressure build-up is univocally related to the normalized damage parameter, κ/κ_L by the following polynomial function (Chiaradonna et al., 2018):

$$r_u = a\left(\frac{\kappa}{\kappa_L}\right)^{b} + (1-a)\left(\frac{\kappa}{\kappa_L}\right)^{d} \tag{5}$$

where a, b and d are curve-fitting parameters (Fig. 1b). Given the proportionality between the number of cycles, N, and the damage parameter, κ (Eq. (5)), any pore pressure change can be expressed as a variation of the normalized number of cycles, N/N_L (see Chiaradonna et al., 2018 for details).

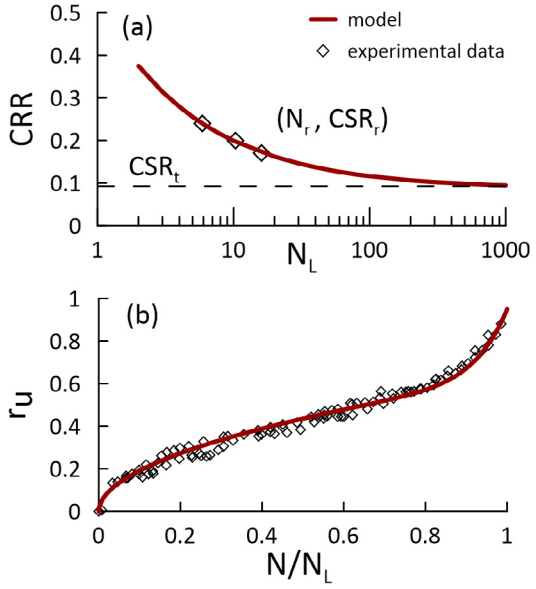

Fig. 1. (a) Cyclic resistance and (b) excess pore pressure ratio curves.

For an irregular shear loading history, expressed as follows:

$$\tau^*(t) = \frac{|\tau(t)|}{\sigma'_0} \tag{6}$$

the damage parameter, κ, can be computed at every time instant as:

$$\kappa(t) = \kappa_0 + d\kappa \tag{7}$$

where κ_0 is the damage cumulated at the last reversal point of the function (τ^*– CSR_t) reached at the time instant t. The parameter κ_0 can be defined as follows:

$$\kappa_0 = \begin{cases} \kappa(t-dt) & \text{if } \dot{\tau}^*(t) = 0 \quad \text{or} \quad \tau^*(t) = CSR_t \\ \kappa_0(t-dt) & \text{if } \dot{\tau}^*(t) \neq 0 \quad \text{or} \quad \tau^*(t) \neq CSR_t \end{cases} \tag{8}$$

i.e., κ_0 is a stepwise function assuming the value of the damage parameter gained at the time step ($t - dt$) every time the stress ratio reaches a local maximum value or when $\tau^* = CSR_t$.

The increment of the damage parameter, $d\kappa$, in the time interval dt is given by:

$$d\kappa = \begin{cases} 0 & \text{if } \tau^*(t) < CSR_t \\ \left[\tau^*_0(t) - \tau(t)\right]^{\alpha} & \text{if } \tau^*(t) \geqslant CSR_t \end{cases} \tag{9}$$

where $\tau^*_0 = \tau^*_{max}$ if $\dot{\tau}^*(t) < 0$ and $\tau^*_0 = CSR_t$ otherwise.

The damage function increases when τ^* overcomes CSR_t, which represents the threshold below which there is no pore pressure build-up. More details about the "PWP model" can be found in Chiaradonna et al. (2018).

It is worth mentioning that the code SCOSSA can also model partially drained condition, since the dissipation of the excess pore pressure is implemented into the code (Tropeano et al., 2019).

3. Proposed calibration procedure

The parameters describing the cyclic resistance curve (α, CSR_r and CSR_t) as well as those characterizing the pore pressure ratio relationship (a, b and d) are usually calibrated on laboratory tests results. Indeed, by so doing, the 'PWP model' has proved effective in simulating well-documented case histories (Tropeano et al., 2019; Chiaradonna et al., 2019). However, in engineering practice, such results are seldom available, and thus, only in-situ tests results can be found.

It is then obvious that semi-empirical methods would be considerably more useful if the calibration relied on the interpretation of in-situ tests (e.g., CPT and SPT) data. In this paper, this procedure is specifically proposed for the model proposed by Chiaradonna et al. (2018), and the steps that have been followed for correlating the model parameters to the in-situ test results are widely described (flow-chart in Fig. 2).

According to Boulanger and Idriss (2014), the results of SPT and CPT are expressed, respectively, in terms of the corrected SPT blowcount, $(N_1)_{60cs}$, and corrected cone tip resistance, q_{c1Ncs}. The corrected cone tip resistance, q_{c1Ncs} is defined as:

$$q_{c1Ncs} = q_{c1N} + \Delta q_{c1N} \tag{10}$$

where:

$$q_{c1N} = C_N \cdot \frac{q_c}{P_a} \tag{11}$$

$$C_N = \left(\frac{P_a}{\sigma'_v}\right)^m \leqslant 1.7 \tag{12}$$

$$m = 1.338 - 0.249 \cdot q_{c1Ncs}{}^{0.264} \tag{13}$$

$$\Delta q_{c1N} = \left(11.9 + \frac{q_{c1N}}{14.6}\right)\exp\left(1.63 - \frac{9.7}{FC+2} - \left(\frac{15.7}{FC+2}\right)^2\right) \tag{14}$$

where q_c in the cone resistance measured during CPT, p_a is the atmospheric pressure and FC is the fine content, i.e., the percentage of soil having particles diameter smaller than 0.075 mm. The value of q_{c1Ncs} must be found by trial and error.

Similarly, the corrected SPT blowcount, $(N_1)_{60cs}$ is defined as:

$$(N_1)_{60cs} = (N_1)_{60} + \Delta(N_1)_{60} \tag{15}$$

where:

$$(N_1)_{60} = C_N \cdot N_{60} \tag{16}$$

C_N is given by equation (12), the exponent m being:

$$m = 0.784 - 0.0768 \cdot (N_1)_{60cs}{}^{0.5} \tag{17}$$

$$\Delta(N_1)_{60} = \exp\left(1.63 + \frac{9.7}{FC+0.01} - \left(\frac{15.7}{FC+0.01}\right)^2\right) \tag{18}$$

where N_{60} is the energy-corrected blow count measured during SPT.

In first step of the flow-chart in Fig. 2, a set of cyclic resistance curves (CRR, N_L) was generated from the empirical relationships between CRR and $(N_1)_{60cs}$ or q_{c1Ncs} proposed by Boulanger and Idriss (2014). These empirical relationships include data obtained from the most recent events where widespread liquefaction was observed (the 2010–2011 Canterbury earthquake sequence in New Zealand and the 2011 Tohoku earthquake in Japan). Then, cyclic strength parameters to define Eq. (2) were defined for all the above-mentioned curves of the dataset using non-linear regression analysis. Finally, the model parameters are expressed as a function of the initial stress state and soil

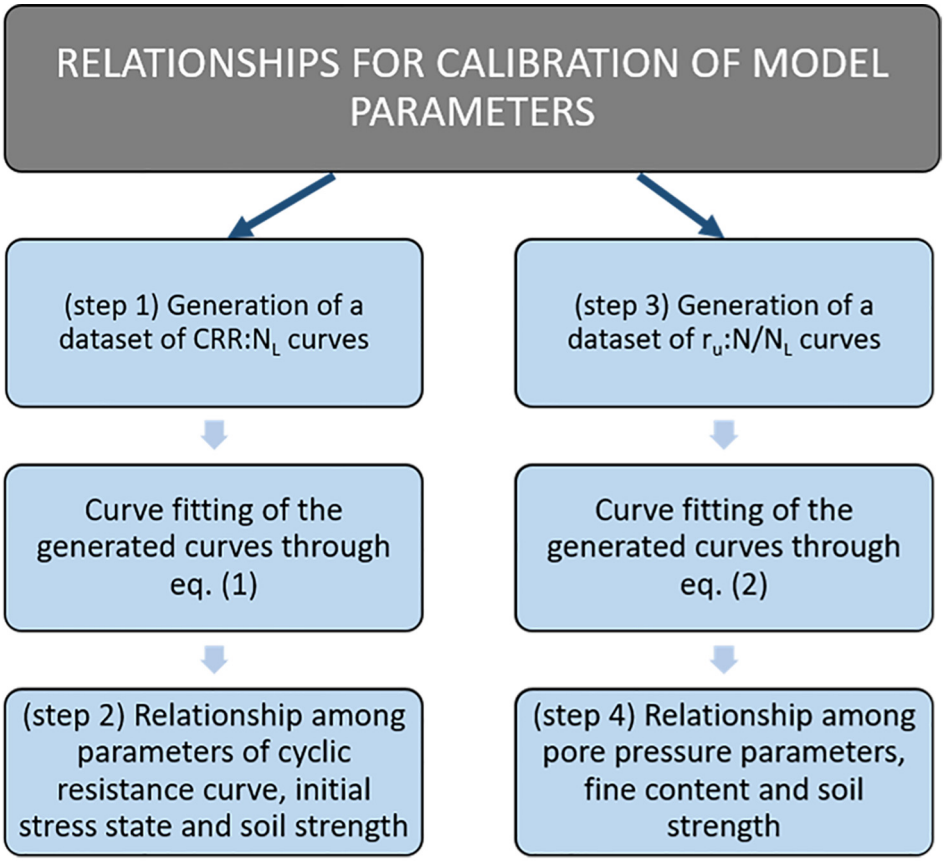

Fig. 2. Flow chart used for defining the relationships for the calibration of the pore water pressure model.

strength evaluated from CPT or SPT, i.e., q_{c1Ncs} or $(N_1)_{60cs}$, respectively (step 2 in Fig. 2).

The same path has been followed for the parameters of the pore pressure ratio curve (Eq. (5)). A dataset of curves (r_u, N/N_L) was generated through the simplified expression proposed by Polito et al. (2008) (step 3 in Fig. 2). Then, the pore pressure parameters to define Eq. (5) were defined for all the above-mentioned curves of the dataset using a non-linear regression analysis. Finally, the model parameters were expressed as a function of fines content and soil strength evaluated from CPT or SPT, i.e., q_{c1Ncs} or $(N_1)_{60cs}$, respectively (step 4).

It is worth highlighting here that the methodology suggested for defining the relationships for use in the calibration of the parameters of the proposed model can be generalized and applied to other simplified pore water pressure models.

3.1. Step 1: Generation of cyclic resistance curves from empirical relationships based on SPT/CPT

Cyclic resistance curves are generated from the empirical relationships proposed by Boulanger and Idriss (2014):

$$CRR_{M=7.5,\sigma'=1} = \exp\left(\frac{(N_1)_{60cs}}{14.1} + \left(\frac{(N_1)_{60cs}}{126}\right)^2 - \left(\frac{(N_1)_{60cs}}{23.6}\right)^3 + \left(\frac{(N_1)_{60cs}}{25.4}\right)^4 - 2.8\right) \quad (19a)$$

$$CRR_{M=7.5,\sigma'=1} = \exp\left(\frac{q_{c1Ncs}}{113} + \left(\frac{q_{c1Ncs}}{1000}\right)^2 - \left(\frac{q_{c1Ncs}}{140}\right)^3 + \left(\frac{q_{c1Ncs}}{137}\right)^4 - 2.8\right) \quad (19b)$$

These allow defining the cyclic resistance ratio (CRR) of the soil characterized by a given value of $(N_1)_{60cs}$ or q_{c1Ncs} at a reference earthquake of 7.5 magnitude and effective overburden stress equal to unity. Eqs. (19a) and (19b) must be corrected to take into account: (i) the overburden stress and (ii) the actual magnitude and duration of the earthquake. The effect of the overburden stress is taken into account by introducing a correction factor K_σ, as in the following equation:

$$K_\sigma = 1 - C_\sigma \cdot \ln\left(\frac{\sigma'_{v0}}{p_a}\right) \leqslant 1.1 \quad (20)$$

where

$$C_\sigma = \frac{1}{18.9 - 2.55\sqrt{(N_1)_{60cs}}} \leqslant 0.3 \quad (21a)$$

$$C_\sigma = \frac{1}{37.3 - 8.27 \cdot q_{c1Ncs}} \leqslant 0.3 \quad (21b)$$

for $(N_1)_{60cs}$ and q_{c1Ncs} respectively.

The effect of magnitude and duration of shaking is taken into account through the earthquake magnitude scaling factor, MSF. The duration of shaking as well as the MSF depend on numerous factors, including earthquake source characteristics, distance from the site to the source, soil profile characteristics, and depth in the soil profile (e.g., Liu et al., 2001, Green and Terri, 2005). The inclusion of all dependencies may not be warranted in practice. The MSF relationship proposed by Boulanger and Idriss (2014) includes a functional dependence on an index of the soil properties, b_b, as follows:

$$MSF = \frac{CSR}{CSR_{M=7.5}} = \left(\frac{N_{M=7.5}}{N}\right)^{b_b} \quad (22)$$

In order to use Eq. (22), the number of equivalent uniform loading cycles for M = 7.5, called $N_{M=7.5}$, and the parameter b_b should be defined.

Fig. 3a shows the geometric mean values of $N_{M=7.5}$ computed by Boulanger and Idriss (2014) for b_b values from 0.06 to 0.40 for a set of 42 motions at category D sites, with peak ground accelerations (PGA) from 0.11 to 0.51 g during M = 7.3–7.6 earthquakes. The geometric mean values for $N_{M=7.5}$ are relatively constant at about 15 for b_b values of 0.2 to 0.4 and then increase rapidly for b_b values progressively lower than about 0.2.

The relationship between $N_{M=7.5}$ and the parameter b_b was described analytically by interpolating the mean curve from Boulanger and Idriss (2014) as proposed by Chiaradonna and Flora (2020):

$$N_{M=7.5} = \frac{18.61 \cdot {b_b}^2 - 3.71 \cdot b_b + 0.38}{{b_b}^2 - 0.091 \cdot b_b + 0.0021} \quad (23)$$

which is the continuous line illustrated in Fig. 3a.

On the other hand, the subsequent path was followed for the definition of the parameter b_b.

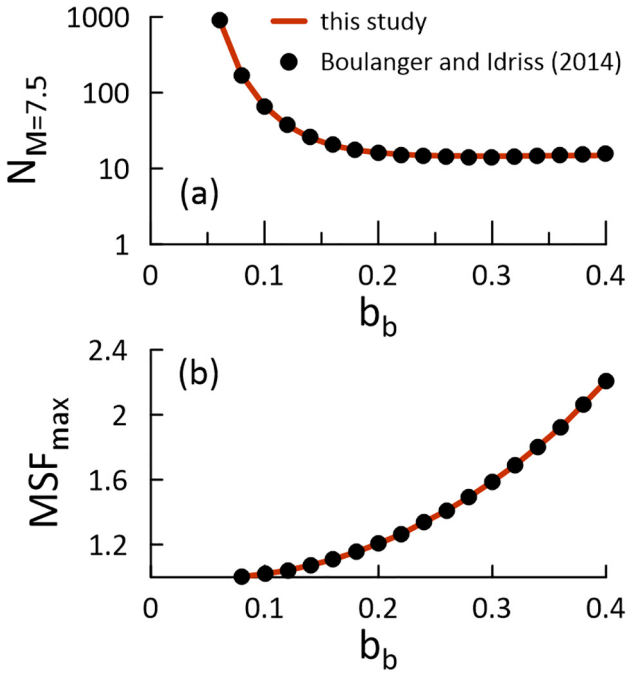

Fig. 3. Variation of (a) $N_{M=7.5}$ and (b) MSF_{max} with the parameter b_b.

Boulanger and Idriss (2014) define the maximum value of the magnitude scaling factor, MSF_{max}, that relates to small magnitude earthquakes. It corresponds to the case where the motion is dominated by a single strong acceleration pulse. They assume that this single pulse scenario is illustrated by ¾ of a cycle at its peak stress and the equivalent number of uniform cycles at 65% of the peak stress is:

$$N_{\min} = \left(\frac{1}{0.65}\right)^{1/b_b} \cdot \left(\frac{3}{4} cycles\right) \tag{24}$$

hence:

$$MSF_{\max} = \left(\frac{N_{M=7.5}}{N_{\min}}\right)^{b_b} \tag{25}$$

Substituting Eqs. (23) and (24) into Eq. (25), the univocal relationship between MSF_{max} and b_b was analytically derived as (Fig. 3b):

$$MSF_{\max} = 0.65\left[\frac{4}{3}\left(\frac{18.61 \cdot {b_b}^2 - 3.71 \cdot b_b + 0.38}{{b_b}^2 - 0.091 \cdot b_b + 0.0021}\right)\right]^{b_b} \tag{26}$$

Boulanger and Idriss (2014) reviewed a significant amount of laboratory test data to compute MSF_{max} for different values of b_b and plotted them versus the equivalent values $(N_1)_{60cs}$ or q_{c1Ncs}, thus obtaining the following equations:

$$MSF_{\max} = 1.09 + \left(\frac{(N_1)_{60cs}}{31.5}\right)^2 \leqslant 2.2 \tag{27a}$$

$$MSF_{\max} = 1.09 + \left(\frac{q_{c1Ncs}}{180}\right)^3 \leqslant 2.2 \tag{27b}$$

Hence, by combining Eqs. (26) and (27a) or (27b), the parameter b_b was finally expressed as a function of $(N_1)_{60cs}$ or q_{c1Ncs}. In this way, the magnitude scaling factor for any number of cycles N is known:

$$MSF = \left(\frac{N_{M=7.5}}{N}\right)^{b_b} \leqslant MSF_{\max} \tag{28}$$

Therefore, to any number of cycles N corresponds a value of MSF (Eq. (28)) and CRR is as a function of N as:

$$CRR = MSF \cdot k_\sigma \cdot CRR_{M=7.5,\sigma'=1} \tag{29}$$

As a result, different cyclic resistance curves were obtained in this work for different values of the effective confining pressure and corrected SPT blow count or CPT cone tip resistance.

A range of $(N_1)_{60cs}$ from 6 to 25 and a range of q_{c1Ncs} from 25 to 150 was considered, because it is the range of SPT and CPT values typical of liquefiable soils. A range, from 50 to 800 kPa, was assumed for the effective confining pressure. An example of the generated curves for an effective overburden stress equal to 50 kPa is reported in Fig. 4.

3.2. Step 2: Calibration of the parameters of the cyclic resistance curve

The calibration procedure of the cyclic strength parameters of the pore water pressure model on the generated

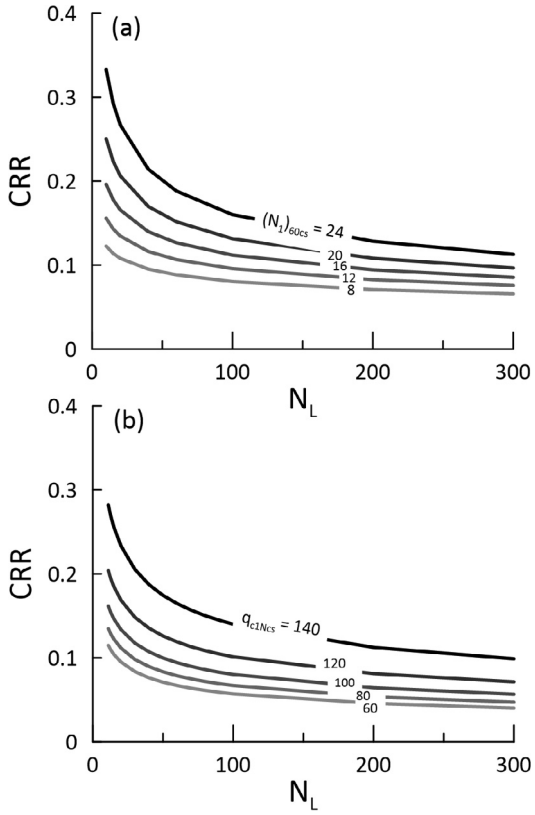

Fig. 4. Set of cyclic resistance curves generated for (a) $(N_1)_{60cs}$ and (b) q_{c1Ncs} for an effective overburden stress equal to 50 kPa.

cyclic resistance curves has been divided into two steps: the first step is related to the calibration of CSR_r, which refers to 15 cycles, while the second one is related to the calibration of CSR_t and α.

CRR values computed for $N_L = 15$ have been plotted as a function of σ'_{v0} and $(N_1)_{60cs}$ or q_{c1Ncs} (Fig. 5a–d).

Hence, the calculated points were interpolated with a polynomial expression, where the coefficients are ruled by σ'_{v0} with a logarithmic function. The following relationships were obtained:

$$CSR_r = x_1 \cdot (N_1)^4_{60cs} + x_2 \cdot (N_1)^3_{60cs} + x_3 \cdot (N_1)^2_{60cs} + x_4 \cdot (N_1)_{60cs} + x_5 \tag{30a}$$

$$CSR_r = y_1 \cdot q^5_{c1Ncs} + y_2 \cdot q^4_{c1Ncs} + y_3 \cdot q^3_{c1Ncs} + y_4 \cdot q^2{}_{c1Ncs} + y_5 \cdot q_{c1Ncs} + y_6 \tag{30b}$$

where

$$x_i = x_{i,1} \cdot \ln\left(\frac{\sigma'_{v0}}{p'_0}\right) + x_{i,2} \text{ for i } = 1,\ 2,\ 3,\ 4,\ 5 \tag{31a}$$

$$y_i = y_{i,1} \cdot \ln\left(\frac{\sigma'_{v0}}{p'_0}\right) + y_{i,2} \text{ for i } = 1,\ 2,\ 3,\ 4,\ 5,\ 6 \tag{31b}$$

with p'_0 equal to the atmospheric pressure. The parameters of expressions (31a) and (31b) were defined through a nonlinear regression analysis and they are reported in Table 1 and Table 2, respectively.

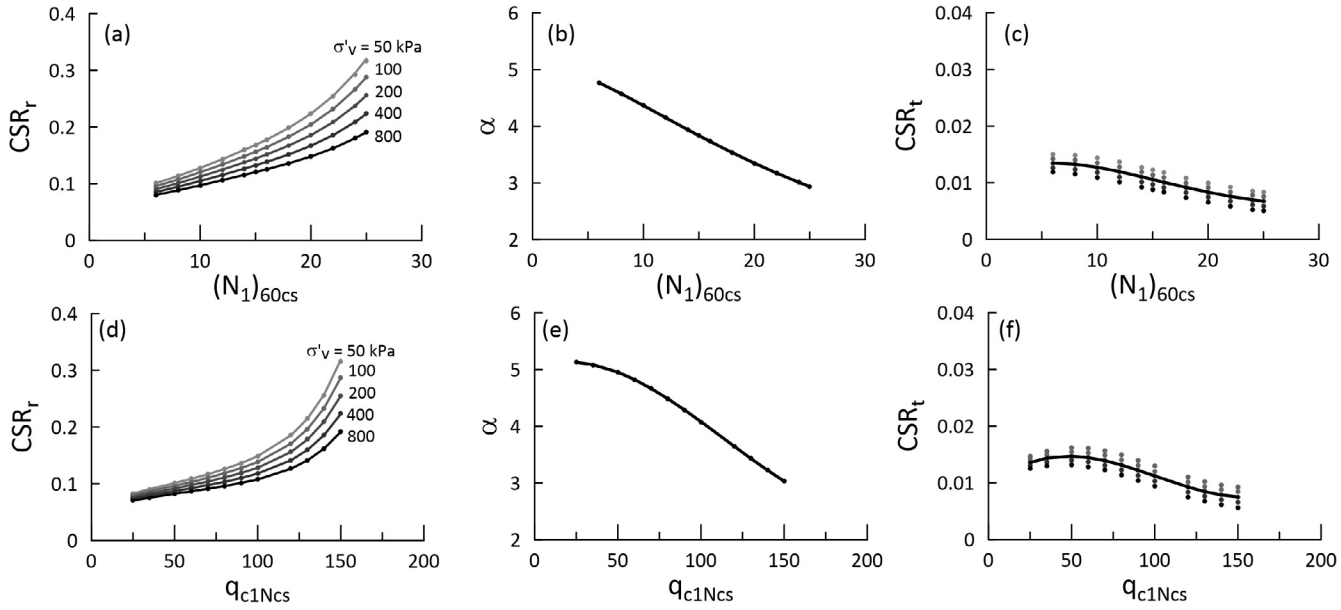

Fig. 5. Parameters of the pore pressure model CSR_r, α and CSR_t as a function of $(N_1)_{60cs}$ and q_{c1Ncs}.

Table 1
Coefficients for computing CSR_r through Eq. (31a).

$x_{1,1}$	$x_{1,2}$	$x_{2,1}$	$x_{2,2}$	$x_{3,1}$	$x_{3,2}$	$x_{4,1}$	$x_{4,2}$	$x_{5,1}$	$x_{5,2}$
−3.07E-07	1.23E-06	1.35E-05	−5.46E-05	−2.57E-04	1.01E-03	1.27E-03	−1.94E-03	−8.45E-03	8.12E-02

Table 2
Coefficients for computing CSR_r through Eq. (31b).

$y_{1,1}$	$y_{1,2}$	$y_{2,1}$	$y_{2,2}$	$y_{3,1}$	$y_{3,2}$
−4.23E-12	1.54E-11	1.40E-09	−4.84E-09	−1.88E-07	6.36E-07
$y_{4,1}$	$y_{4,2}$	$y_{5,1}$	$y_{5,2}$	$y_{6,1}$	$y_{6,2}$
1.17E-05	−4.05E-05	−4.26E-04	1.87E-03	1.38E-03	5.00E-02

With reference to the calibration of the parameter α, governing the steepness of the cyclic resistance curve, Boulanger and Idriss (2014) relate the slope of the curve to the corrected number of blow count or cone tip resistance, so the parameter α is ruled only by $(N_1)_{60cs}$ or q_{c1Ncs}. As shown in Fig. 5b,e, the relationship is almost linear. However, a cubic regression function was adopted since it has a coefficient of determination, R^2, equal to 1.

Two regression curves were generated, as a funcion of $(N_1)_{60cs}$ or q_{c1Ncs}, respectively:

$$\alpha = x_6 \cdot (N_1)_{60}^3 + x_7 \cdot (N_1)_{60}^2 + x_8 \cdot (N_1)_{60} + x_9 \quad (32a)$$

$$\alpha = y_7 \cdot q_{c1Ncs}^3 + y_8 \cdot q_{c1Ncs}^2 + y_9 \cdot q_{c1Ncs} + y_{10} \quad (32b)$$

CSR_t was defined as the shear stress ratio, CRR, of the generated curves corresponding to one million of cycles.

The threshold shear stress ratio, CSR_t, was plotted in Fig. 5c,f as a function of $(N_1)_{60cs}$ and q_{c1Ncs} for different values of effective stress, σ'_{v0}.

Due to the small values of shear stress ratio, the effect of σ'_{v0} was neglected and the following expression was adopted for modelling CSR_t:

$$CSR_t = x_{10} \cdot (N_1)_{60}^4 + x_{11} \cdot (N_1)_{60}^3 + x_{12} \cdot (N_1)_{60}^2 + x_{13} \cdot (N_1)_{60} + x_{14} \quad (33a)$$

$$CSR_t = y_{11} \cdot q_{c1Ncs}^4 + y_{12} \cdot q_{c1Ncs}^3 + y_{13} \cdot q_{c1Ncs}^2 + y_{14} \cdot q_{c1Ncs} + y_{15} \quad (33b)$$

The x_i and y_i coefficients of α and CSR_t expressions were computed using an optimization procedure based on the non-linear regression method, and are reported in Table 3.

3.3. Step 3: Generation of pore pressure build-up curves from empirical relationships based on cyclic laboratory tests

A dataset of pore pressure build-up curves was generated through a simplified expression reported by Polito et al. (2008). They adopted the simplified model for predicting pore water pressure build-up originally developed by Booker et al. (1976), where the pore pressure ratio, r_u, is a function of the ratio of the number of applied uniform cycles, N/N_L, and of the coefficient β via the expression:

Table 3
Coefficients of the relationships from (32a)–(33b).

x_6	x_7	x_8	x_9	x_{10}	x_{11}	x_{12}	x_{13}	x_{14}
6.50E-05	−2.25E-03	−7.92E-02	5.31E +00	−3.73E-08	3.67E-06	−1.16E-04	1.03E-03	1.08E-02
y_7	y_8	y_9	y_{10}	y_{11}	y_{12}	y_{13}	y_{14}	y_{15}
8.50E-07	−2.90E-04	1.12E-02	5.01E + 00	−2.19E-12	1.27E-08	−3.72E-06	2.69E-04	8.95E-03

$$r_u = \frac{2}{\pi}\arcsin\left(\frac{N}{N_L}\right)^{1/2\beta} \tag{34}$$

Fig. 6 shows the upper and lower bounds of residual excess pore pressure proposed by Lee and Albaisa (1974), and the curve related to $\beta = 0.7$, which is the value recommended for clean sands by Booker et al. (1976).

Based on 145 cyclic triaxial tests on sands mixed with various amount of non-plastic silt, Polito et al. (2008) computed the parameter β of equation (34) as a function of fine content in percent, *FC*, (particles smaller than 0.075 mm), relative density as a percentage, *Dr*, and the cyclic stress ratio, *CSR*, as follows:

$$\beta = c_1 \cdot FC + c_2 \cdot Dr + c_3 \cdot CSR + c_4 \tag{35}$$

where c_1, c_2, c_3, c_4 are regression coefficients. For FC < 35%, β increases with increasing *FC* and *Dr* and it is relatively independent of *CSR*, so that the contribution of *CSR* can be neglected. In this case, Eq. (35) simplifies to:

$$\beta = 0.01166 \cdot FC + 0.007397 \cdot Dr + 0.5058 \tag{36}$$

where the coefficients were computed by Polito et al. (2008) through a nonlinear regression analysis of the experimental results and *Dr* and *FC* are still expressed in percentage.

Considering Eqs. (34) and (36), a set of pore water pressure ratio curves was defined in the range of *FC* from 0 to 30% and *Dr* from 20 to 80%. An example of the generated curves for a fine content equal to 0 and 35% is reported in Fig. 7.

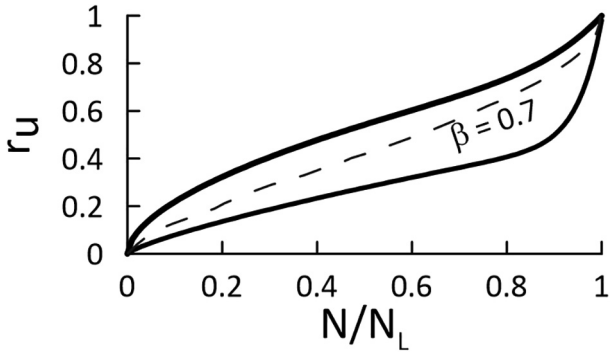

Fig. 6. Upper and lower bounds of residual excess pore pressure generation as function of cycle ratio, N/N_L, and average curve for $\beta = 0.7$.

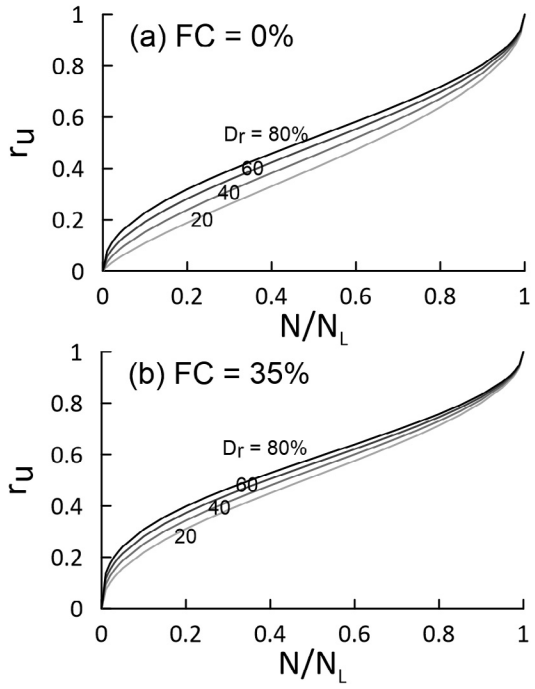

Fig. 7. Set of pore pressure curves generated for (a) *FC* = 0 and (b) *FC* = 35%.

3.4. Step 4: Calibration of the parameters of pore pressure build-up

The pore pressure parameters, i.e., *a, b, d* in Eq. (5), were defined for all the generated curves of the dataset (Fig. 7) using non-linear regression analysis. The obtained values were then plotted as a function of fine content and relative density of soil (Fig. 8) and analytical relationships to model the observed trends were proposed, such as the following.

Analytically, parameter *a* can be computed as:

$$a = a_{11} \cdot FC + a_{21} \cdot Dr^4 + a_{22} \cdot Dr^3 + a_{23} \cdot Dr^2 + a_{24} \cdot Dr + a_{25} \tag{37}$$

While the exponents, *b* and *d,* can be computed as:

$$b = (b_{11} \cdot Dr^2 + b_{12} \cdot Dr + b_{13}) \cdot \exp[FC \cdot (b_{21} \cdot Dr^2 + b_{22} \cdot Dr + b_{23})] \tag{38}$$

$$d = d_{11} \cdot \exp[d_{12} \cdot Dr + FC \cdot (d_{21} \cdot Dr^2 + d_{22} \cdot Dr + d_{23})] \tag{39}$$

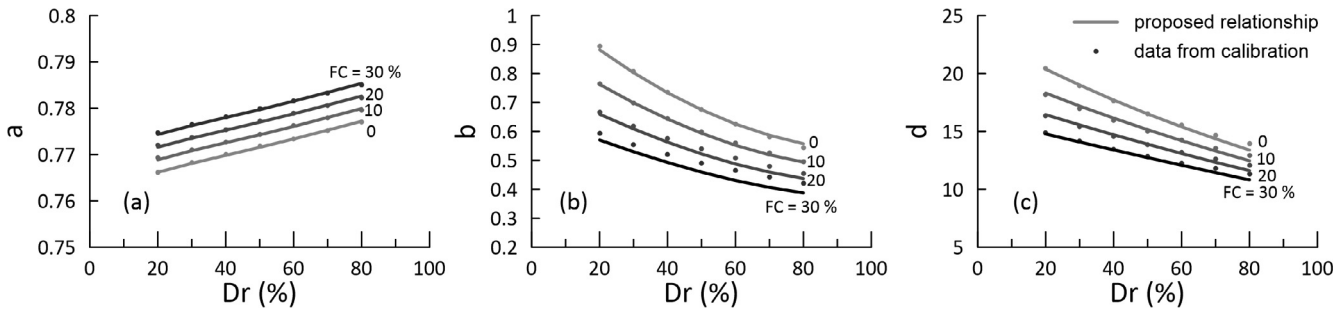

Fig. 8. Parameters (a) a, (b) b and (c) d of the Eq. (5) plotted as function of the fine content, FC and the relative density, Dr, and interpretated by the proposed relationships (continous lines).

Table 4
Regression coefficients of the parameter a (Eq. (37)).

a_{11}	a_{21}	a_{22}	a_{23}	a_{24}	a_{25}
0.000272	−4.0E-10	9.0E-08	−7.0E-06	4.0E-04	0.7603

Table 5
Regression coefficients of b (Eq. (38)).

b_{11}	b_{12}	b_{13}	b_{21}	b_{22}	b_{23}
5.0E-05	−0.0104	1.0695	−6.0E-07	1.0E-04	−0.0163

Table 6
Regression coefficients of d (Eq. (39)).

d_{11}	d_{12}	d_{21}	d_{22}	d_{23}
23.433	−0.007	−3E-07	−9E-05	−0.0124

The regression coefficients of Eqs. (37), (38) and (39) are reported in Tables 4, 5 and 6.

The use of the above-described relationships requires the availability of data about the relative density, Dr, and fine content, FC. The latter is usually available while Dr can be estimated using one of the empirical correlations with SPT or CPT results (e.g., Kulhawy and Mayne, 1990).

4. Evaluation of the proposed approach through case histories

The described procedure is applied to two real cases, where downhole and surface acceleration records were available. Both the considered sites are the results of reclamation works where no specific soil treatments were used to induce densification of the granular soils.

4.1. Port Island

Port Island is an artificial island constructed at the South of Kobe City, Osaka Bay, Japan (Fig. 9a). This island was constructed in two phases. During the first phase, a 436 ha area was reclaimed. In the second phase, the island was extended southward by reclaiming 319 additional hectares (Fig. 9). A decomposite granite soil known as 'Masado', transported from the nearby Rokko Mountains, was used in the first reclamation phase, while sandstone, mudstone, and tuff were employed in the second phase (Shibata et al., 1996).

A vertical array was installed in the northern area of Port Island in October 1991 (Iwasaki and Tai, 1996), including triaxial accelerometers at the surface as well as at depths of 16 m, 32 m, and 83 m from the ground level. No piezometers were installed at the array site.

On January 17, 1995, at 5:46 AM, the Hyogoken-Nanbu earthquake with a local magnitude of 7.2 struck the southern part of Hyogo Prefecture. The epicenter was 15 km north of Awaji Island (Fig. 9a), and the hypocenter depth was located 14.3 km below sea level (Shibata et al., 1996).

Liquefaction was widespread throughout Port Island; especially in the reclamation area created in the first phase: settlements of 20 cm were observed on average, with peak values exceeding 50 cm. The ejection of liquefied materials was observed on Port Island for nearly one hour after the earthquake (Shibata et al., 1996).

The downhole acceleration array recorded the main shock at different depths. The horizontal acceleration was not amplified at the ground surface, because the liquefaction of the soil shallower than 16 m resulted in the deamplification of the higher frequency components (Fig. 10a–c).

In this work, only the shallow liquefied layer of the vertical array was considered in the numerical simulation, imposing the bedrock at 16 m, where a downhole accelerometer was located (Fig. 10). The NS component of the earthquake recorded at 16 m depth was used as input motion and applied as inside motion to the rigid bedrock (Fig. 10c). It is worth noting that the depth of the seismic bedrock was unknown at the site.

The considered soil column consists of Masado soil, which is a known liquefiable soil.

Fig. 11a shows the grain size distribution curve of the Masado soil (up to 150 mm), a well-graded soil which contains a fairly large portion of gravel (about 55%).

The shear wave velocity, V_S, and SPT profiles at the array site (Fig. 10d,e), as reported by Ishihara et al. (1996), were used in the definition of the geotechnical model.

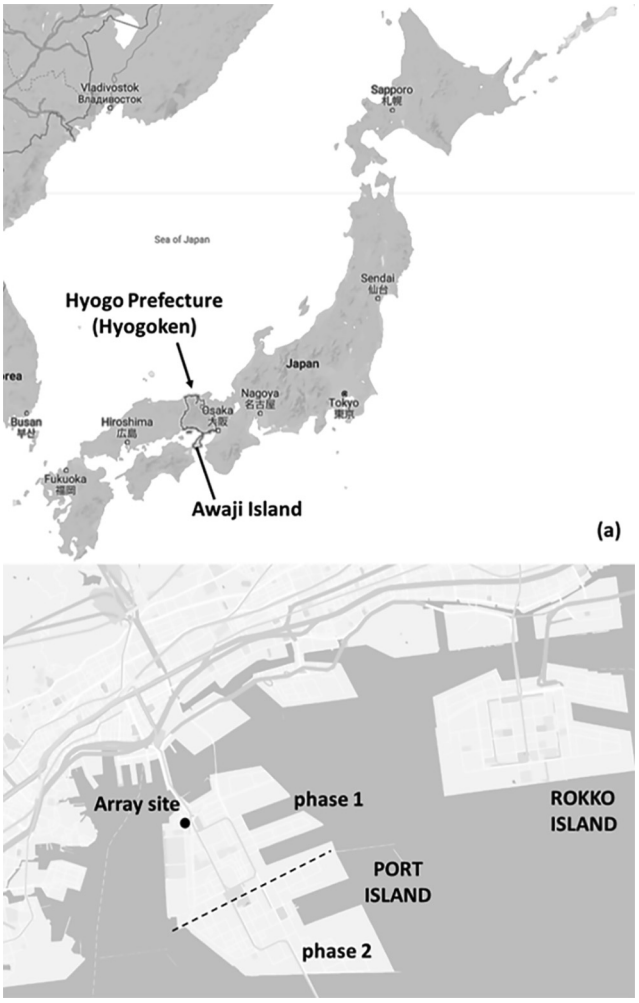

Fig. 9. Location of Hyogoken in Japan (a) and focus on Port Island with the location of the vertical array (b). The dashed line separates the part of the island constructed during the first and the second phase.

The number of blow counts was corrected in order to calibrate the pore water pressure model: an average N_{60} value was calculated and then corrected for the energy ratio:

$$N_{60} = N_{SPT} \cdot \frac{ER_m}{60} \tag{40}$$

where N_{SPT} is the measured blow count, ER_m the measured delivered energy ratio (%) and N_{60} the blow count for an energy ratio of 60%. The energy ratio for the N_{SPT} values in Fig. 10 was assumed to be 75%, based on typical practice in Japan, and then used to calculate N_{60}, as already assumed also by other authors (Ziotopoulou, 2010). Then, the obtained N_{60} was further corrected according to Eq. (16) and finally $(N_1)_{60cs}$ was obtained since no correction was applied for the fines content (FC $\approx$ 5% and thus $(N_1)_{60} = (N_1)_{60cs}$).

The parameters of the PWP model for Masado soil were defined according to the proposed procedure, i.e., the cyclic resistance curve was defined as described in Section 3.2, and the pore pressure build-up parameters were computed through the procedure described in Section 3.4, where the relative density, Dr, was estimated as a function of $(N_1)_{60}$, according to Idriss and Boulanger (2008):

$$D_r = \sqrt{\frac{(N_1)_{60}}{46}} \tag{41}$$

The resulting curves of the pore water pressure model are plotted in Fig. 11c, d.

Finally, the non-linear and damping behaviour of the Masado soil was characterised adopting the normalized shear modulus G/G_0 and damping ratio, D, vs. the shear strains, γ, curves proposed by Kokusho and Esashi (1981) for gravelly soils (Fig. 11b).

Since the liquefaction phenomena lasted more than one hour, perfect undrained conditions could be assumed during the earthquake and the dissipation was neglected in the analysis.

Fig. 12 reports the results of total (no pore pressure build-up is simulated) and effective stress analyses together with the record at surface, in terms of time history and response spectra of acceleration.

The time history of accelerations computed by total stress analysis is characterized by higher amplitude and frequency content respect to the recorded accelerations (Fig. 12a). Instead, the effective stress analysis was able to predict the reduction of both amplitude and frequency content (Fig. 12b). The usefulness of the effective stress analysis is also confirmed by the comparison among the numerical simulations and the recorded acceleration response spectra (Fig. 12c). The comparison shows that the total stress analysis significantly overestimates the spectral accelerations over the whole range of periods, whereas the effective stress analysis well captures the measured PGA and identified the range of periods where the maximum amplifications occur, although spectral accelerations were underestimated in this range. This confirms the importance of taking the pore pressure build-up into account in order to correctly predict both the shift of frequency content towards lower values and the reduction of spectral amplitudes due to liquefaction.

4.2. Treasure Island

Treasure Island is a 400 acre man-made island immediately northwest of the Yerba Buena Island, a rock outcrop in San Francisco Bay (Fig. 13a). It was constructed in 1936–37 for activities celebrating the construction of the Golden Gate and San Francisco-Oakland Bay Bridges (Graizer, 2011).

Treasure Island was constructed by hydraulic and clamshell dredging. A perimeter rock dike was built in two to four stages on a bed of coarse sand. The dike acted as a retaining system for the sands that were pumped or placed inside. The structure is thus essentially an upstream constructed hydraulic fill (Zhang et al., 2002).

During the 1989 Loma Prieta earthquake, liquefaction-related phenomena, were evident at many locations across

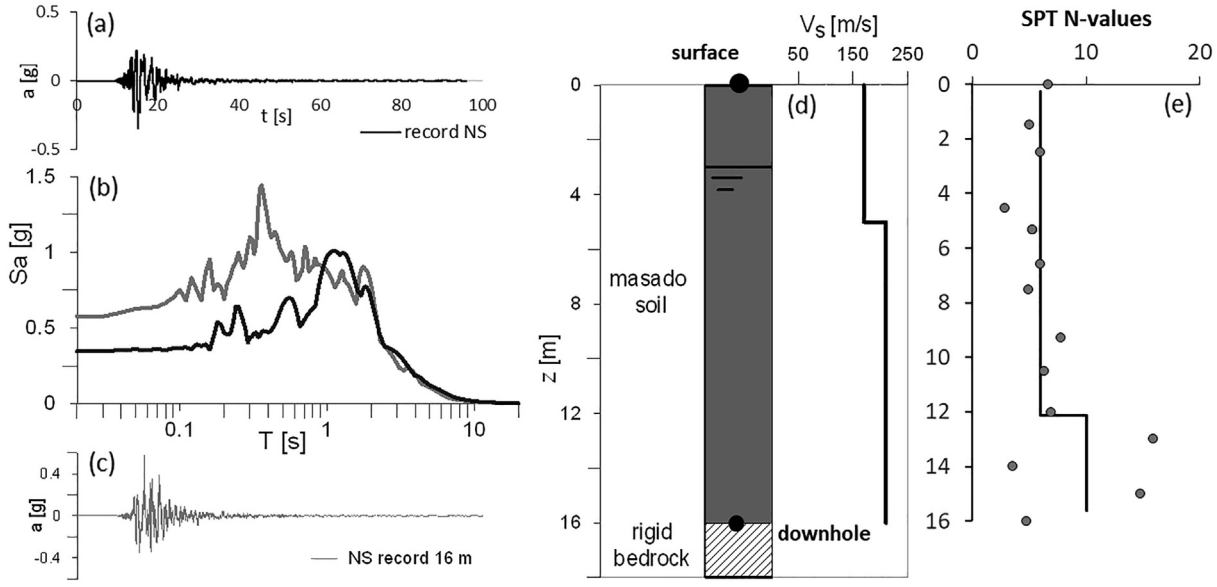

Fig. 10. Recorded acceleration, a, vs. time, t (a) at surface and at (c) 16 m depth and (b) acceleration response spectra, Sa, (5% damping); (d) soil column and profiles of shear wave velocity, V_S and (e) blow count of SPT, N_{SPT} (Ishihara et al., 1996).

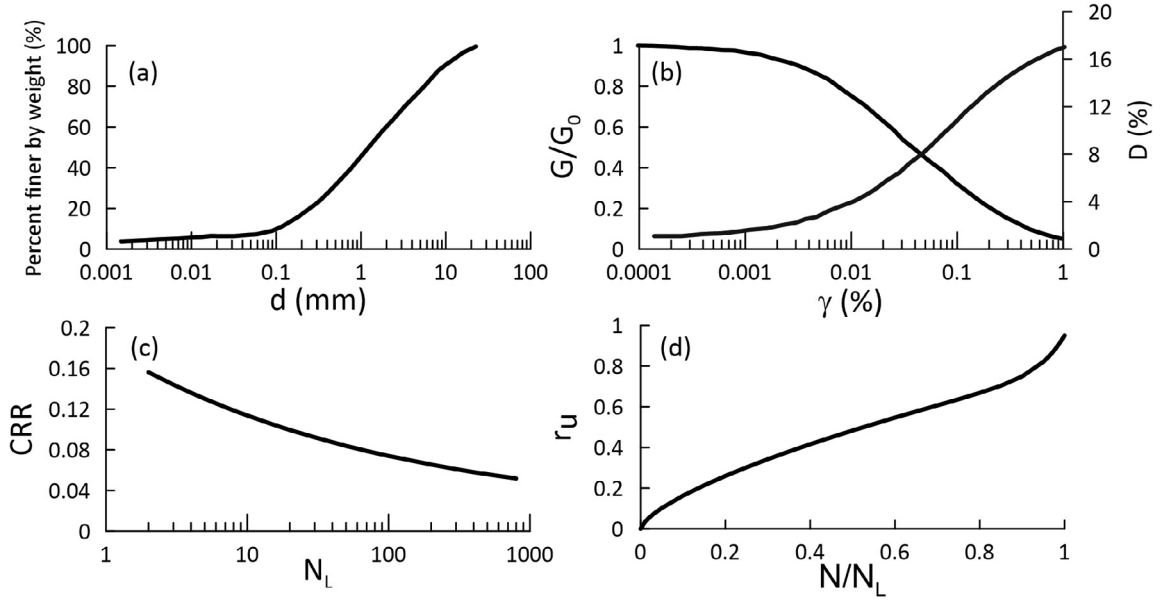

Fig. 11. Masado soil: (a) grain size distribution (modified after Nagase et al. 1996), (b) normalized shear modulus and damping ratio vs shear strain (modified after Kokusho and Esashi, 1981), (c) cyclic resistance curve and (d) pore pressure relationship from SPT profile.

the island, including sand boils, ground surface settlements and lateral spreading movements (Hryciw et al., 1991; Power et al., 1998). The buildings and underground utilities were damaged by the ground settlements and lateral displacements.

The peak acceleration recorded at the fire station on Treasure Island during the earthquake (Fig. 13b) was 0.16 g (Hryciw et al., 1991) and past studies have shown that the intensity of ground shaking did not vary greatly at different places on the island (Hryciw et al., 1991; Power et al., 1998).

The recorded accelerations at Treasure Island and on Yerba Buena Island (E-W) clearly reveal the effects of site amplification (Fig. 13b,c). Moreover, a drop in the high-frequency content can be observed in the Treasure Island record after 14 s, which has been recognized as a typical effect of liquefaction (Kramer et al., 2011).

The soils at Treasure Island may be grouped into four broad categories: the fill material (hydraulic fill), recent bay sediments (Young Bay Mud), native shoal sands (fine to medium sand) and older bay sediments (old Bay Clay) (Fig. 14a). The shear wave velocity profile was reported

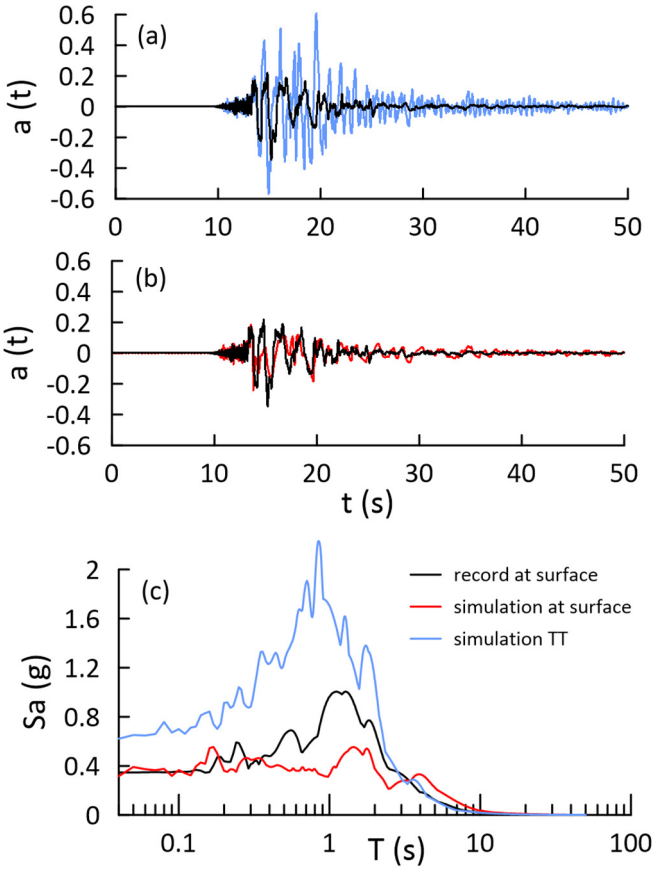

Fig. 12. Port Island: comparison between time histories of recorded and simulated acceleration from (a) total stress analysis (TT) and (b) effective stress analysis and (c) among recorded and simulated acceleration response spectra (5% damping) at the surface.

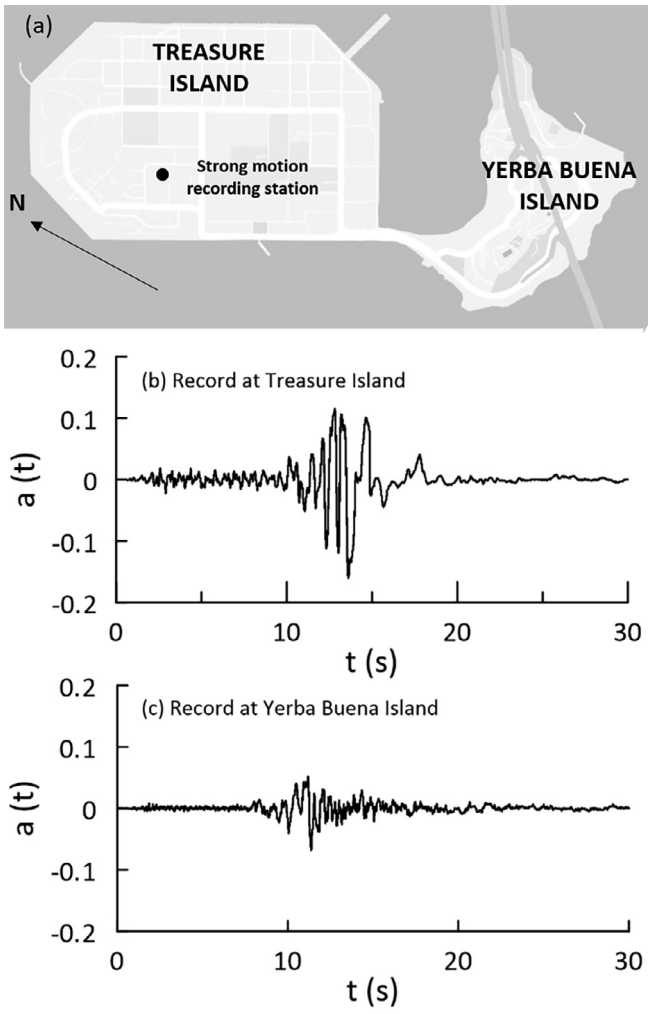

Fig. 13. Treasure Island and Yerba Buena Island (a), the recorded motion of the Loma Prieta Earthquake at Treasure Island (b) and Yerba Buena Island (c).

by Graizer (2011) based on the P-S suspension logging performed in a 122 m deep downhole (Fig. 14c), revealing that the bedrock depth was located at 88 m depth from the ground level (Fig. 14).

The EW component of the acceleration record at Yerba Buena Island was used as input motion in the numerical simulations, and was applied as outcrop motion at the bedrock depth (Fig. 13c).

Liquefaction involved the hydraulic fill, while the other layers are assumed to be not liquefiable. The fill material is predominantly sand with varying degrees of gravel, silt, and clay. Even though the hydraulic fill is a very heterogeneous layer (Fig. 15a), a mean percentage of fine content equal to 15% was assumed in the calibration of the pore water pressure model. A CPTU until 25 m depth from the ground level (Fig. 13b) was carried out close to the recorded station, as reported by Pass (1994) and the results of the test were used to define a corrected cone tip resistance, q_{c1Ncs}, profile. This latter was used to define the parameters of the cyclic strength of the soil, as described in Section 3.2 (Fig. 5) and to estimate the relative density, *Dr* according to Idriss and Boulanger (2008):

$$D_r = 0.478 \cdot q_{c1Ncs}{}^{0.264} - 1.063 \quad (42)$$

The obtained value of relative density, in conjunction with the fine content, was finally used to calculate the model parameters *a*, *b*, *d* (Fig. 8). The curves coming from the proposed calibration procedure of the pore water pressure model, are reported in Fig. 15c,d.

For the sake of simplicity, the shear modulus degradation and damping curves were defined as grouping the sand formations (hydraulic fill and sand layers) and the clayey formations (young and old clay bay). In particular, the upper bound curves proposed by Seed and Idriss (1970) were assumed for the sandy layers, while the curves obtained by laboratory tests on young bay mud samples by Sun et al. (1988) were assumed for the clayey formations (Fig. 15b).

The results of the effective stress analysis are reported in Fig. 16, in terms of acceleration time history and response spectrum, where they are compared with the record at the surface and analysis result in total stress. The computed spectral ordinates in effective stress are underestimates for periods lower than 1 s, while they are overestimated

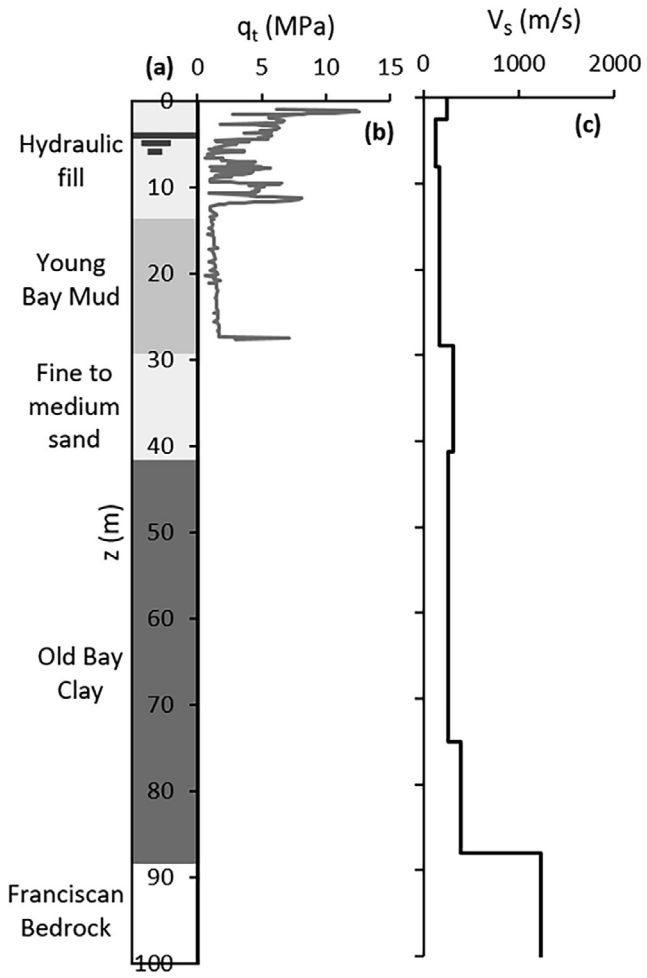

Fig. 14. (a) Soil profile of Treasure Island (b) CPTU (Pass, 1994) and (c) V_S profiles (Graizer, 2011).

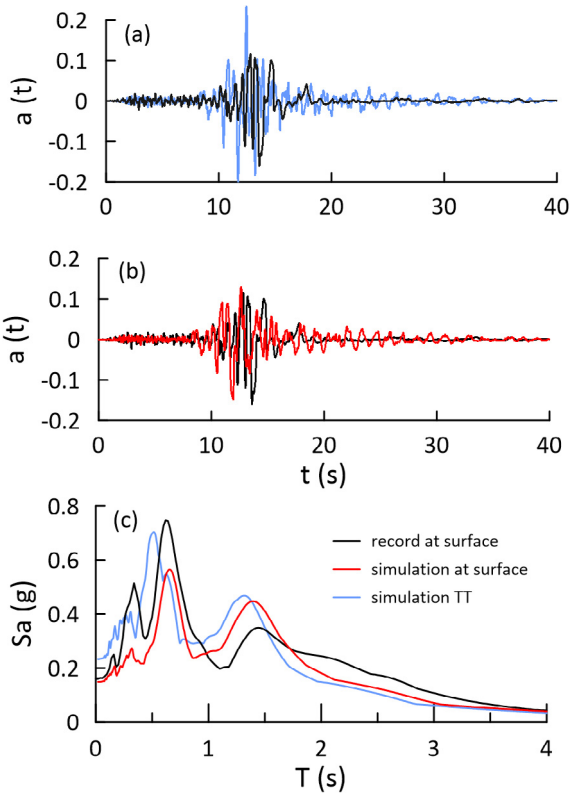

Fig. 16. Treasure Island: comparison between time histories of recorded and simulated acceleration from (a) total stress analysis (TT) and (b) effective stress analysis and (c) among recorded and simulated acceleration response spectra (5% damping) at the surface.

between 1 and 1.8 s; however, the overall agreement between recorded and predicted spectrum is satisfactory in terms of both PGA and predominant period, especially if compared to the analysis result in total stress.

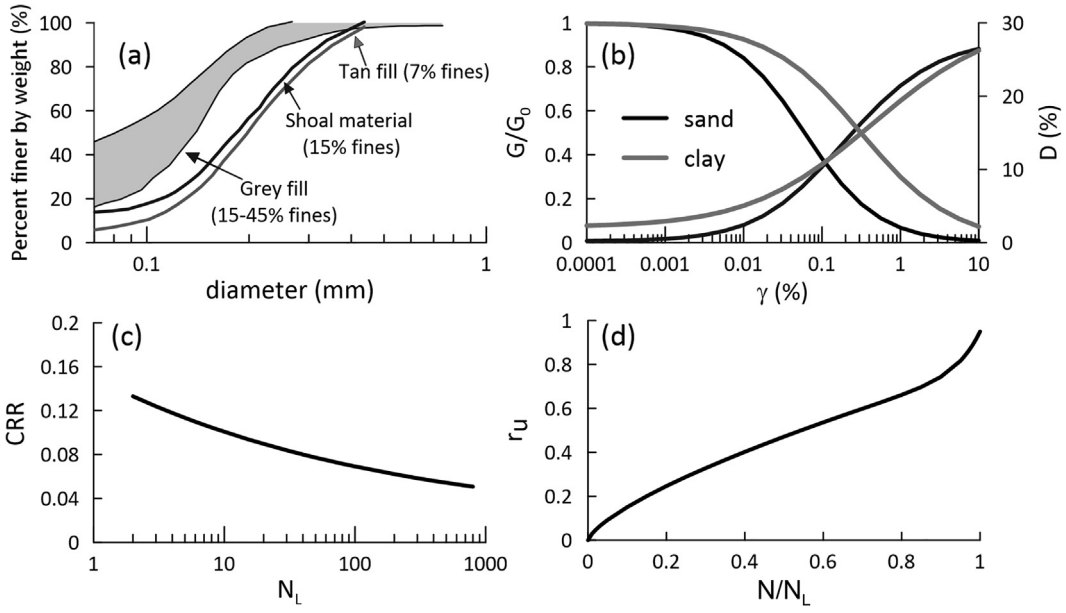

Fig. 15. Soil properties: (a) grain size distribution of hydraulic fill (modified after Pass, 1994), (b) normalized shear modulus and damping ratio vs shear strain, (c) cyclic resistance curve and (d) pore pressure relationship for hydraulic fill defined on CPT profile.

5. Discussion and conclusions

In this paper, a calibration procedure is proposed for defining the parameters of a pore water pressure model necessary to carry out a non-linear, effective stress numerical simulations in 1-D condition (Chiaradonna et al., 2018) on the basis of in situ test results, thus overcoming the limitation caused by the typical lack of laboratory data in current engineering practice.

The adopted pore water pressure model requires the definition of two semi-empirical curves: the cyclic resistance curve and the pore pressure ratio curve. The parameters of the first curve (CRR-N_L) have been computed as a function of the effective stress state and of SPT or CPT results. The parameters of the second curve ($r_u - N/N_L$) have been defined as a function of the fines content and relative density, the latter estimated from either SPT or CPT. This method allows the pore water pressure model to be easily calibrated directly on the basis of the results of in-situ tests. The methodology followed to define the calibration relationships (Figs. 5 and 8) can be generalized and applied to other simplified pore water pressure models.

The proposed procedure has been validated by comparing the simulation results with the recorded seismic site response in two well known and documented case histories. The quality of the prediction firstly depends on the ability of the code to evaluate the soil response in terms of generation of excess pore water pressure, which is obtained with limited effort in terms of calculation and calibration of the model.

The comparison with the experimental results was satisfactory, demonstrating that the procedure leads to a reliable prediction notwithstanding the simplicity in the calibration procedure. It was also shown that the proposed procedure is more effective than a simple analysis of total stresses in predicting the recorded spectrum of acceleration, which highly overestimates the maximum accelerations and underestimates the critical periods because of its inability to take the isolating effect of liquefaction into account. However, some limitations should be recognized by the use of the proposed calibration procedure: in particular, caution should be taken with the cyclic resistance curve for very loose soils. For such soils, the generated dataset underestimates the cyclic resistance ratio for a small number of cycles (Fig. 4), resulting in a conservative prediction of pore pressure increments for moderate intensity shakings.

Acknowledgments

This work was carried out as part of the European project Horizon 2020 – Assessment and Mitigation of liquefaction potential across Europe: A holistic approach to protect structures infrastructures for improved resilience to earthquake-induced liquefaction disasters – "LIQUEFACT" (grant agreement No 700748).

The authors would like to thank Professor S.L. Kramer from the University of Washington for providing useful suggestions in the calibration process of the pore water pressure model.

References

Beaty, M., Byrne, P.M., 1998. An effective stress model for predicting liquefaction behavior of sand. In Vol. 1 of Geotechnical Earthquake Engineering and Soil Dynamics III, 766–777. Reston, VA: ASCE.

Booker, J.R., Rahman, M.S., Seed, H.B., 1976. GADFLEA- A computer program for the analysis of pore pressure generation and dissipation during cyclic or earthquake loading. Earthquake Engineering Center, University of California, Berkeley.

Boulanger, R.W., Idriss, I.M., 2014. CPT and SPT liquefaction triggering procedures. Report No UCD/GCM-14/01. University of California at Davis, California, USA.

Boulanger, R.W., Ziotopoulou, K., 2015. PM4Sand (Version 3): A sand plasticity model for earthquake engineering applications. Rep. No. UCD/CGM-15/01. Davis, CA: Center for Geotechnical Modeling. Univ. of California.

Chiaradonna, A., Flora, A., 2020. On the estimate of seismically-induced pore water pressure increments before liquefaction. Geotechnique Lett. https://doi.org/10.1680/jgele.19.00032.

Chiaradonna, A., Tropeano, G., d'Onofrio, A., Silvestri, F., 2019. Prediction of non-linear soil behaviour in saturated sand: a loosely coupled approach for 1D effective stress analysis. Proc. of the 7th International Conference on Earthquake Geotechnical Engineering, 7ICEGE, Rome (Italy), June 2019, ISBN: 978-0-367-14328-2 (Hbk) (eBook).

Chiaradonna, A., Tropeano, G., d'Onofrio, A., Silvestri, F., 2018a. Development of a simplified model for pore water pressure build-up induced by cyclic loading. Bullet. Earthquake Eng. https://doi.org/10.1007/s10518-018-0354-4.

Chiaradonna, A., Tropeano, G., d'Onofrio, A., Silvestri, F., 2018b. Interpreting the deformation phenomena of a levee damaged during the 2012 Emilia earthquake. Soil Dyn. Earthquake Eng. https://doi.org/10.1016/j.soildyn.2018.04.039.

Chiaradonna, A., Tropeano, G., d'Onofrio, A., Silvestri, F., 2016. A simplified method for pore pressure buildup prediction: from laboratory cyclic tests to the 1D soil response analysis in effective stress conditions. Procedia Eng. 158, 302–307. https://doi.org/10.1016/j.proeng.2016.08.446.

Chiaradonna, A., 2016. Development and assessment of a numerical model per non-linear coupled analysis on seismic response of liquefiable soils. PhD Dissertation. University of Napoli 'Federico II'.

Dafalias, Y.F., Manzari, M.T., 2004. Simple plasticity sand model accounting for fabric change effects. J. Eng. Mech. 130 (6), 622–634. https://doi.org/10.1061/(ASCE)0733-9399(2004) 130:6(622).

Elgamal, A., Yang, Z., Parra, E., 2002. Computational modeling of cyclic mobility and post-liquefaction site response. Soil Dyn. Earthquake Eng. 22 (4), 259–271. https://doi.org/10.1016/S0267-7261(02)00022-2.

Graizer, V., 2011. Treasure Island geotechnical array – case study for site response analysis. University of California Santa Barbara, California, USA.

Green, R.A., Terri, G.A., 2005. Number of equivalent cycles concept for liquefaction evaluations—revisited. J. Geotech. Geoenviron. Eng. ASCE 131 (4), 477–488.

Hashash, Y.M.A., Phillips, C., Groholski, D.R., 2010. Recent advances in non-linear site response analysis. Proc. Fifth. Int. Conf. Recent Adv. Geotech. Earthq. Eng. Soil. Dyn. 29 (6), 1–22.

Hashash, Y.M.A., Musgrove, M.I., Harmon, J.A., Groholski, D.R., Phillips, C.A., Park, D., 2016. DEEPSOIL 6.1, User Manual. Board of Trustees of University of Illinois at Urbana-Champaign, Urbana, IL.

Hryciw, R.D., Shewbridge, S.E., Rollins, K.M., McHood, M., Homolka, M., 1991. Soil Amplification at Treasure Island during the Lorna Prieta Earthquake. In Proceedings of the Second International

Conference on Recent Advances in Geotechnical Earthquake Engineering and Soil Dynamics, St. Louis, Missouri, Paper No. LP20.
Idriss, I.M., Boulanger, R.W., 2008. Soil liquefaction during earthquakes. Monograph MNO-12. Earthquake Engineering Research Institute, Oakland, CA.
Ishihara, K., Yasuda, S., Nagase, H., 1996. Soil characteristics and ground damage. Special Issue Soils Found., 109–118.
Iwasaki, Y., Tai, M., 1996. Strong motion records at Kobe Port Island. Special Issue Soils Found., 29–40.
Kondner, R.L., Zelasko, J.S., 1963. Hyperbolic stress-strain formulation of sands. Proceedings of the 2nd Pan-American conference on soil mechanics and foundation engineering. Sao Paulo, Brazil. Associação Brasileira de Mecânica dos Solos.
Kramer, S.L., Hartvigsen, A.J., Sideras, S.S., Ozner, P.T., 2011. Site response modelling in liquefiable soil deposits. University of California Santa Barbara, California, USA.
Kokusho, T., Esashi, Y., 1981. Cyclic triaxial test on sands and coarse materials. Proceedings of the 10th International Conference on Soil Mechanics and Foundation Engineering, Stockholm, 1, pp. 673–679.
Kulhawy, F.H., Mayne, P.W., 1990. Manual on estimating soil properties for foundation design. Report EL-6800, Electric Power Research Institute, Palo Alto, p. 306 www.epri.com.
Lee, K.L., Albaisa, A., 1974. Earthquake induced settlements in saturated sands. J. Geotech. Eng. Div. 100 (4), 387–406.
Lee, M.K.W., Finn, W.D.L., 1978. DESRA-2 Dynamic Effective Stress Response Analysis of soil deposits with energy transmitting boundary including assessment of liquefaction potential. Soil Mech Series. Department of Civil Engineering, University of British Columbia, Canada.
Liu, A.H., Stewart, J.P., Abrahamson, N.A., Moriwaki, Y., 2001. Equivalent number of uniform stress cycles for soil liquefaction analysis. J. Geotech. Geoenviron. Eng. ASCE 127 (12), 1017–1026.
Matasovic, N., Hashash, Y.M.A., 2012. Practices and procedures for site-specific evaluations of earthquake ground motions: a synthesis of highway practice. National Cooperative Highway. Research Project Synthesis Report No. 428. Transportation Research Board, Washington, DC, p. 79.
Matasovic, N., Ordonez, G.A., 2011. DMOD 2000: A computer program for nonlinear seismic response analysis of horizontally layered soil deposits, earthfill dams and solid waste landfills. GeoMotions LLC, Lacey, WA.
Matasovic, N., Vucetic, M., 1993. Cyclic characterization of liquefiable sands. J. Geotech. Eng. ASCE 119 (11), 1805–1822.
Nagase, H., Yasuda, S., Tsujino, S., Shinji, R., Yanagihata, T., 1996. Liquefaction strength characteristics of overconsolidated sand samples. In Proceedings of the Eleventh World Conference on Earthquake Engineering, Acapulco, Mexico, 1996, p. 1098.
Pass, D.G., 1994. Soil characterization of the soil of the deep accelerometer site at Treasure Island, San Francisco, California. Master Degree Thesis. University of New Hampshire.
Phillips, C., Hashash, Y.M.A., 2009. Damping formulation for non linear 1D site response analyses. Soil Dyn. Earthquake Eng. 29 (7), 1143–1158.
Polito, C.P., Green, R.A., Lee, J., 2008. Pore pressure generation models for sands and silty soils subjected to cyclic loading. J. Geotech. Geoenviron. Eng. ASCE 134 (10), 1490–1500.
Power, M.S., Egan, J.A., Shewbridge, S.E., deBecker, J., Faris, J.R., 1998. Analysis of liquefaction-induced damage on Treasure Island. The Loma Prieta, California, Earthquake of October 17, 1989 - Liquefaction. USGS survey professional paper 1551-B.
Prevost, J.H., 1985. A simple plasticity theory for frictional cohesionless soils. Soil Dyn. Earthquake Eng. 4 (1), 9–17. https://doi.org/10.1016/0261-7277(85)90030-0.
Ramirez, J., Barrero, A.R., Cheng, L., Dashti, S., Ghofrani, A., Taiebat, M., Arduino, P., 2018. Site response in a layered liquefiable deposit: evaluation of different numerical tools and methodologies with centrifuge experimental results. J. Geotech. Geoenviron. Eng. 144 (10), 04018073. Available at: http://ascelibrary.org/doi/10.1061/%28ASCE%29GT.1943-5606.0001947.
Seed, H.B., Idriss, I.M., 1970. Soil moduli and damping factors for dynamic response analysis. Report No EERC 70–10. University of California, Berkeley, California, USA.
Shibata, T., Oka, F., Ozawa, Y., 1996. Characteristics of ground deformation due to liquefaction. Special issue Soil Found., 65–79
Sun, J.I., Golesorkhi, R., Seed, H.B., 1988. Dynamic moduli and damping ratios for cohesive soils. Report No UCB/EERC-88/15. University of California at Berkeley.
Tropeano, G., Chiaradonna, A., d'Onofrio, A., Silvestri, F., 2016. An innovative computer code for 1D seismic response analysis including shear strength of soils. Géotechnique 66 (2), 95–105.
Tropeano, G., Chiaradonna, A., d'Onofrio, A., Silvestri, F., 2019. Numerical model for non-linear coupled analysis on seismic response of liquefiable soils. Comput. Geotech. 105, 211–227. https://doi.org/10.1016/j.compgeo.2018.09.008.
Zhang, G., Robertson, P.K., Brachman, R.W.I., 2002. Estimating liquefaction-induced ground settlements from CPT for level ground. Canadian Geotech. J. 39, 1168–1180.
Ziotopoulou, K., 2010. Evaluating model uncertainty against strong motion records at liquefiable sites. Master of Science in Civil and Environmental Engineering. University of California, Davis, USA.